Proceedings of the 16th European Turbomachinery Conference (ETC16)
Turbomachinery, Fluid Dynamics and Thermodynamics,
March 24-28, 2025; Hannover, Germany

Flutter Analysis of the ECL5 Open Fan Testcase Using Harmonic Balance

Christian Frey*[1], Stéphane Aubert[2], Pascal Ferrand[2], and Anne-Lise Fiquet[2]

[1]German Aerospace Center (DLR), Institute of Propulsion Technology, Linder Höhe, 51147 Cologne, Germany
[2]Univ Lyon, Ecole Centrale de Lyon, CNRS, Univ Claude Bernard Lyon 1, INSA Lyon, LMFA, UMR 5509, 69130, Ecully, France

Abstract

This paper presents the flutter analysis of the UHBR Open Fan Testcase ECL5 for an off-design point at part speed and focuses on the second eigenmode which has a strong torsional character near the blade tip. Recent studies by Pagès et al., using a time-linearised solver, showed strong negative damping for an operating point on the 80% speedline close to the maximal pressure ratio. This was identified as a phenomenon of convective resonance; for a certain nodal diameter and frequency the blade vibration is in resonance with convective disturbances that are linearly unstable.

In this work, a nonlinear frequency domain method (harmonic balance) is applied to the problem of aerodynamic damping prediction for this off-design operating point. It is shown that, to obtain plausible results, it is necessary to treat the turbulence model as unsteady. The impact of spurious reflections due to numerical boundary conditions is estimated for this case. While a strong negative damping is not predicted by the analysis presented here, we observe a particularly high sensitivity of the aerodynamic response with respect to the turbulence model formulation and the frequency for certain nodal diameters. The combination of nodal diameter and frequency of maximal sensitivities are interpreted as points near resonance. We recover from these near-resonance points convective speeds and compare them to studies of the onset of nonsynchronous vibrations of the ECL5 fan at part speed conditions.

Keywords: Aeroelasticity, CFD, Flutter, ECL5, Harmonic Balance.

1 Introduction

With the aim of higher efficiencies and reduced weight, there is an ongoing trend towards fan designs with higher bypass and lower pressure ratios as well as composite materials. For such fans, the goals of lower weights and high aerodynamic performance compete with aeroelastic stability, especially near stall conditions. Critical fan blade vibrations near stall can be due to various causes:

- Flutter bite due to stall flutter.
- Rotating stall, i.e., rotating cells of stalled flow which cause high unsteady pressures, thereby exciting blade eigenmodes [1].
- Non-synchronous vibrations (NSV) due to the interaction of a self-excited circumferentially convected aerodynamic disturbance which locks in with some eigenmode [2, 3].

Whereas for NSV the involved physical mechanisms are still the subject of active research, fan stall flutter can nowadays be regarded as well understood: the unsteady flow response due to a small blade vibration causes unsteady pressure forces which increase the vibrational energy leading to a positive feedback loop. The aerodynamic work per cycle which is added to the structure and the related damping quantitiy must therefore be estimated at an early design phase in order to ensure flutter free fans [4]. Though qualitatively well understood, flutter bite is nevertheless difficult to predict with computational methods for several reasons:

- Flutter bite occurs typically for off-design conditions with complex flow structures in the blade tip region. Established CFD methods, in particular turbulence models, bring with them a high degree of uncertainty for these flow conditions.
- Flutter onset is often related to the interaction with an acoustic mode which is cut-off downstream, but cut-on in the intake where it is partly reflected [5]. The reflection mechanisms have to be predicted rather accurately for a reliable flutter analysis.
- The CFD-based flutter analysis of turbomachinery components (not just fans) is highly sensitive to spurious numerical reflections at inlets and outlets.

To advance the understanding of aeroelastic instability mechanisms, Ecole Centrale de Lyon, in cooperation with the Von Karman Institute for Fluid Dynamics, has initiated an extensive research program. This included a newly designed fan module, the so-called ECL5, which was developed with the aim of an open test case that is representative of modern low-speed composite fans. The ECL5 has been investigated for a couple of years with a strong focus on non-synchronous coupling mechanisms between aerodynamics, acoustics and structure dynamics within the European Clean Sky 2 project CATANA[1] (Composite Aeroelastics and Aeroacoustics).

Although both experimental and computational research in the CATANA project has a strong focus on NSV, the design of the ECL5 was also thoroughly investigated with respect to potential flutter onset. During these studies, Pagès et al. [6]

*Corresponding author: christian.frey@dlr.de

[1]catana.ec-lyon.fr

found that, at 80% rotational speed, the aerodynamic damping of the second eigenmode becomes negative for the nodal diameter of 5, causing a V-shaped spike in the damping curve. The minimal aerodynamic damping ratio was about -5.6% and in apparent contradiction to both experiments and computational studies with time-domain methods [7]. The authors of [6] suspected that the high negative damping could indicate a lock-in with a counter-rotating disturbance. However, the exact reasons for the unusual value remained unclear.

The aims of this paper are the following:

- The reference results in [6] are used to validate the Harmonic Balance (HB) method of DLR's turbomachinery flow solver TRACE for fan flutter at near stall conditions.
- Regarding the nodal diameter 5, this paper clarifies whether the above-mentioned spike in the damping curve occurs for linearised methods only.
- The HB method is, in principle, capable of predicting highly nonlinear unsteady dynamics. We will use HB here to shed some light on the nonlinear fluid-structure interaction process.

The paper is organized as follows: after introducing the numerical method and configuration, a standard flutter analysis using HB is performed and several influence parameters are investigated. First, the impact of the turbulence model formulation as well as the numerical boundary conditions is studied. Then a frequency sensitivity study is performed to localise resonance frequencies for several nodal diameters. Then the question of nonlinear effects is addressed with simulations including the zeroth and higher harmonics.

2 Configuration and Numerical Setup

The test case studied in this work is the open UHBR Fan ECL5/CATANA. Details about the geometry can be found in [6]. It comprises a fan section with 16 fan blades as well as an OGV domain with 31 vanes, see Fig. 1. Note that the computational domain used here does not include the air intake. Otherwise, the mesh is identical to the one used by Fiquet et al. [8]. All simulations below are carried out for a computational domain with the inlet boundary placed at an axial position that is marked with a red dashed line in Fig. 1. To investigate the impact of possible numerical reflections we consider simulations with the long domain.

The rotational speed is 80% of the design speed, i.e., 8800 rpm and the operating point corresponds to $26\,\mathrm{kg\,s^{-1}}$

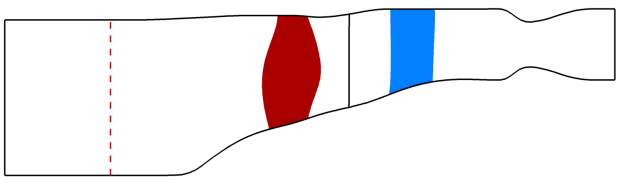

Figure 1: Computational domain of the fan and OGV. Unless otherwise stated the red line marks the inlet boundary.

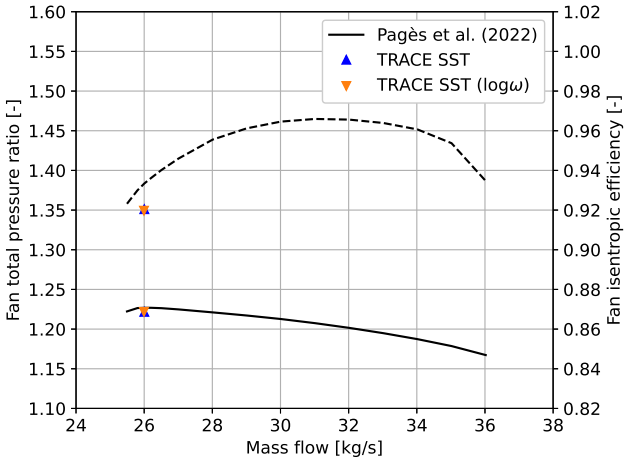

Figure 2: Operating point and 80% speedline data from [6]

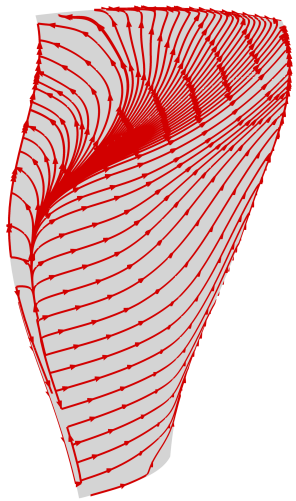

Figure 3: Streaklines on suction side

and is shown in Fig. 2. For this operating point, the streaklines along the fan suction side, as predicted by the steady solver of TRACE are shown in Fig. 3. As was observed by Pagès et al. [6], a considerable back flow zone exists in the upper part of the blade.

Throughout this work, Menter's SST turbulence model [9] with the stagnation point anomaly fix by Kato and Launder [10] has been used. We consider both the original ω- and the $\log\omega$-formulations. Fig. 4 shows the radial velocity at 95% channel height, normalised by the upstream axial velocity, for the two formulations. As can be seen, the radial velocity contours are nearly identical. The choice of the formulation, at least for this mesh, has thus a minor impact on the tip leakage flow. Moreover, we infer from Fig. 2 that it neither has an effect on the overall performance at the operating point under investigation.

2.1 Flutter Analysis

In this paper, the aerodynamic response for the second eigenmode and all nodal diameters except $N_\mathrm{d} = \pm 1$ is studied.

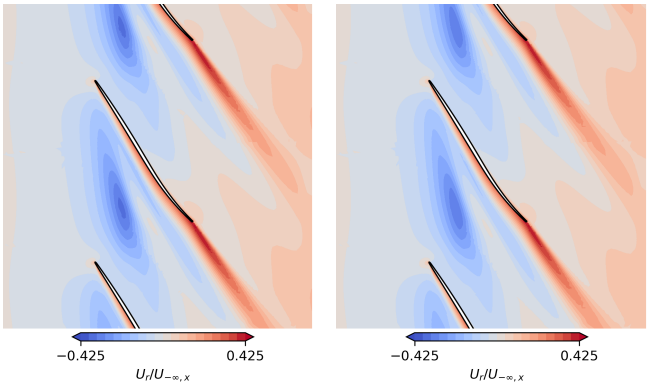

(a) k-ω (b) k-log ω

Figure 4: Radial velocity at 95% channel height.

Apart from the exceptional nodal diameter 1, the mode shapes were found to be nearly independent of the nodal diameter in a previous study [6]. The mode shape corresponding to $N_d = 5$ is used here for all other nodal diameters. The eigenfrequencies, in turn, depend on the nodal diameter and are identical to the ones in [6]. The displacement amplitude of the mode shape is shown in Fig. 5. A maximal displacement of 0.05 mm

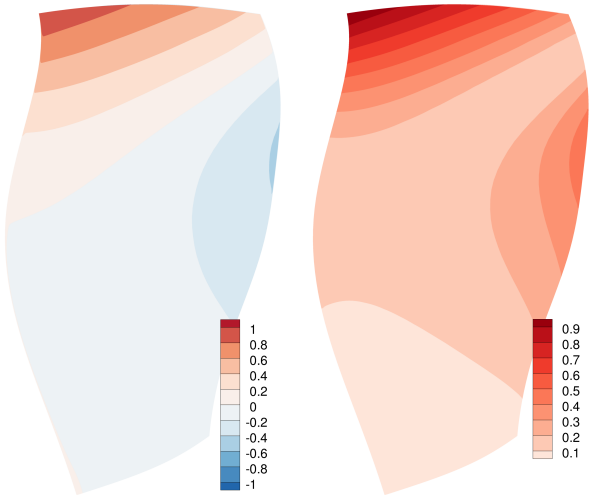

(a) Normal displacement (b) Displacement norm

Figure 5: Displacement vector norm and face normal component of second eigenmode.

is taken here as the standard amplitude. When discussing nonlinear effects we will vary this amplitude by a factor of 0.1 and 10.

As is common practice for turbomachinery flutter analysis, we employ the so-called energy method, i.e., our analysis will look at the flow response in terms of two global parameters: the aerodynamic damping ratio

$$\zeta = \frac{-\operatorname{Re} W_{\mathrm{cyc}}}{4\pi E}, \tag{1}$$

and the aerodynamic stiffness ratio

$$\kappa = \frac{\operatorname{Im} W_{\mathrm{cyc}}}{4\pi E}, \tag{2}$$

where $E = \frac{1}{2}\omega^2 m$ is the modal energy, ω the angular eigenfrequency, and m the modal mass of the eigenmode which is identical to the one used by Pagès et al. [6]. W_{cyc} is the complex modal work per cycle added to the structure,

$$W_{\mathrm{cyc}} = \int_0^{2\pi/\omega} \overline{\dot{q}_{\mathrm{mod}}(t)} F_{\mathrm{mod}}(t)\, dt, \tag{3}$$

with the modal displacement given by $q_{\mathrm{mod}}(t) = e^{\mathbf{i}\omega t}$ and the instantaneous modal force

$$F_{\mathrm{mod}}(t) = \int_\Gamma \psi^H(x)\, p(t,x)\, \vec{n}(t,x)\, dS(x). \tag{4}$$

Here, Γ is the vibrating blade surface and ψ is the mode shape. So the damping is positive if the real part of W_{cyc} (active part) is negative and the fluid extracts energy from the vibration.

2.2 Numerical Method

All CFD simulations are performced with the flow solver TRACE which is DLR's inhouse solver for turbomachinery and has been developed for about three decades in close cooperation with MTU Aero Engines. In this work, the spatial discretisation is based on a cell-centred finite volume scheme, using Roe's flux [11] in combination with a second-order MUSCL extrapolation [12] and a van-Albada type limiter [13].

The unsteady simulation method employed here is the harmonic balance (HB) method [14] which has been extended and validated for flutter analysis [15, 16]. Several studies have shown that in many cases, instead of adopting the so-called frozen turbulence approach, one should rather apply the harmonic balance method to the turbulence equations as well [17, 18].

The harmonic balance method for K higher harmonics is to approximate the time-periodic flow response by a truncated Fourier series,

$$q(t) = \operatorname{Re} \sum_{k=0}^{K} \widehat{q}_k e^{\mathbf{i}k\omega t}. \tag{5}$$

Using this convention for the definition of the complex harmonics, the harmonic balance equation for the k-th harmonic is

$$\mathbf{i}k\omega \widehat{(Vq)}_k + \widehat{VR(q)}_k = 0, \tag{6}$$

where q is the vector of conservative states in each cell, V is the vector of time-dependent cell volumes [15]. The harmonics in Eq. (6) are computed using discrete Fourier transforms again which amounts to looping over N_{sp} sampling points. Here, to reduce the aliasing error, the number of sampling points is always set to $N_{\mathrm{sp}} = 4K + 1$ sampling points. Since the residual R is a nonlinear function of the flow state, the equations for the harmonics are coupled. For the pseudotime marching approach that is used to solve the HB equations, the reader is referred to [14].

At the inlet and outlet boundaries all harmonics, including

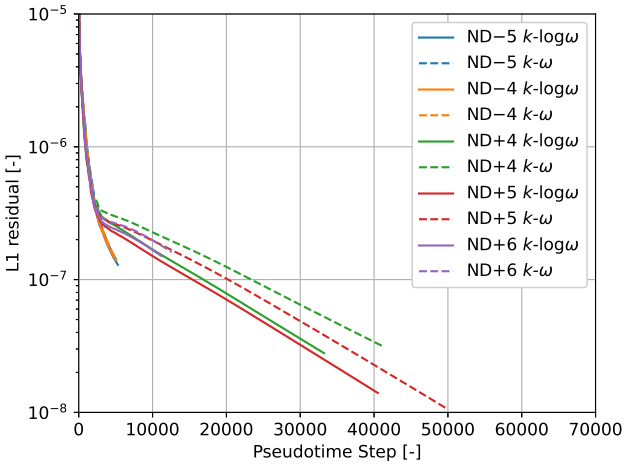

(a) L1 residual

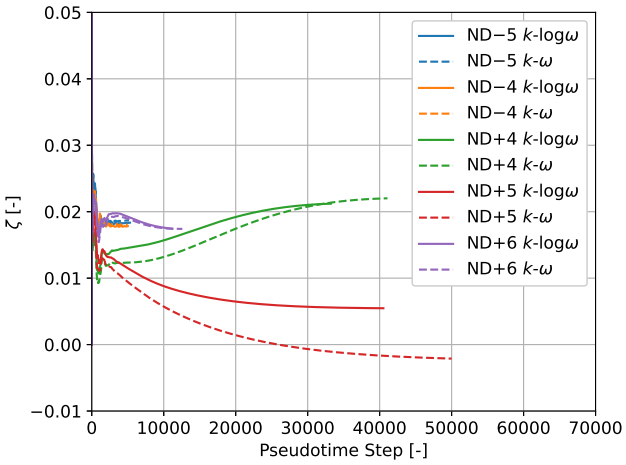

(b) Damping Ratio

Figure 6: Convergence for various nodal diameters

the mean flow, are treated with 2D nonreflecting boundary conditions. At the rotor-stator interface, these nonreflecting boundary conditions are also applied to all circumferential modes that do not match with a corresponding mode in the neighbouring domain.

Below, results from HB setups which resemble time-linearised approaches in that the mean flow is frozen and $K = 1$ are discussed. In this case, Eq. (6) is solved only for the first harmonic. It should be noted though that the resulting equation is still non-linear. Such a setup will be denoted by H1 as opposed to H0..K which denotes a setup where all K higher harmonics and the mean flow are solved for. The configurations that were run for this study are summarized in Table 1.

For the HB simulations in this work, the CFL number was set to 10. When the relative variation of both the damping and the stiffness ratios was less than 1% over 2500 pseudotime steps the simulation was terminated. The convergence of the H1 setups for the nodal diameters 4, 5 and 6 is shown in Fig. 6 and compared to that for the negative nodal diameters -5 and -4. For the positive nodal diameters, the convergence is much slower. The aerodynamic damping for $N_\mathrm{d} = 5$, for instance, exhibited a slow drift over a long period rather than a damped oscillation as was observed for negative nodal diameters.

3 Turbulence Model

As has been shown in recent studies [18], the use of a so-called log ω-formulation can be particularly beneficial for flutter analyses in terms of both robustness and mesh sensitivity, in particular when used with harmonic balance methods. This is mainly due to the fact that temporal variations are resolved with a finite number of Fourier harmonics. High gradients in signals can lead to Gibbs-like phenomena. These high oscillations, in turn, can cause the turbulent dissipation rate to take unphysically small or even negative values, leading to numerical instabilities.

Regarding the convergence speed, Fig. 6 shows that the simulations with the log ω-formulation were somewhat faster than the standard implementation of the SST model. In contrast, simulations with the frozen turbulence assumption were unsuccessful in terms of the residual reduction and did not give physically meaningful results, see Fig. 7.

We conclude that the turbulence model quantities should, for this operating point, always be modelled as unsteady. Note that TRACE also has a time-linearized method [19] which, however, is based on the frozen-eddy viscosity hypothesis and is therefore of limited use for this operating point.

In the following, the two formulations for a setup with just one harmonic (and frozen mean) are compared. Figure 8 shows the resulting values of the aerodynamic damping and

Table 1: Numerical setups used in this work.

TM formulation	harmonics	f/f_eigen	vib amp [mm]	domain
$k-\omega$	H1	1	0.05	fan
$k-\log\omega$	H1	1	0.05	fan
$k-\log\omega$	H1	1	0.005	fan
$k-\omega$	H1	1	0.05	fan + OGV
$k-\omega$	H1	1	0.05	fan (long intake)
$k-\omega$	H1	0.8 to 1.2	0.05	fan
$k-\log\omega$	H0..5	1	0.05	fan + OGV(H0)
$k-\log\omega$	H0..5	1	0.5	fan + OGV(H0)
$k-\log\omega$	H0..5	1	0.05	fan + OGV(H0)
$k-\log\omega$	H0..10	1	0.05	fan + OGV(H0)

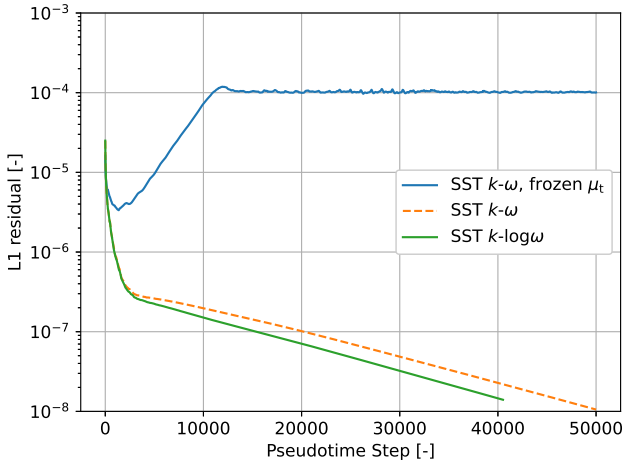

(a) L1 residual

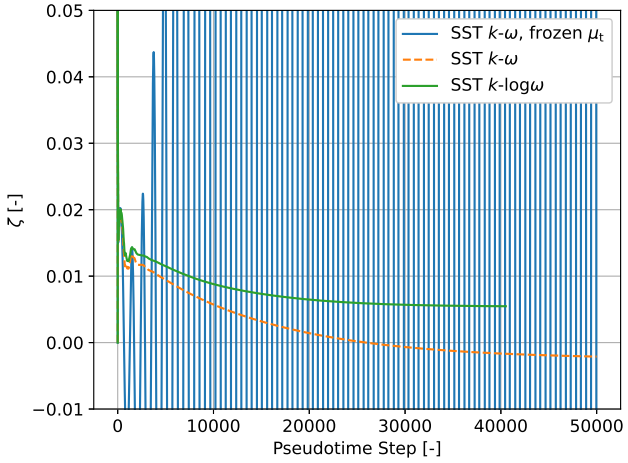

(b) Damping Ratio

Figure 7: Convergence for $N_d = 5$ for ω and $\log\omega$ formulations of SST model as well as for simulation with frozen turbulence.

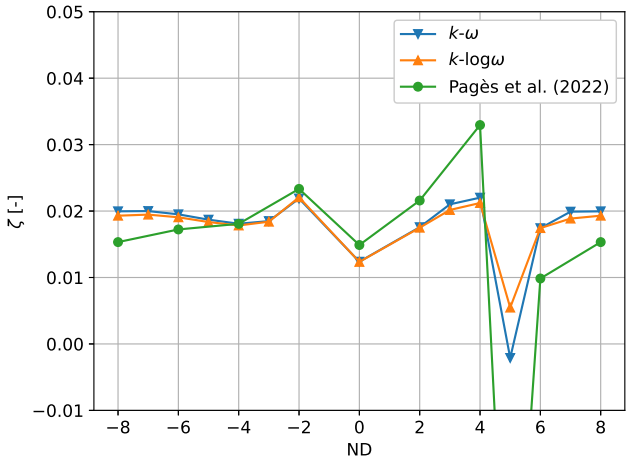

(a) Damping

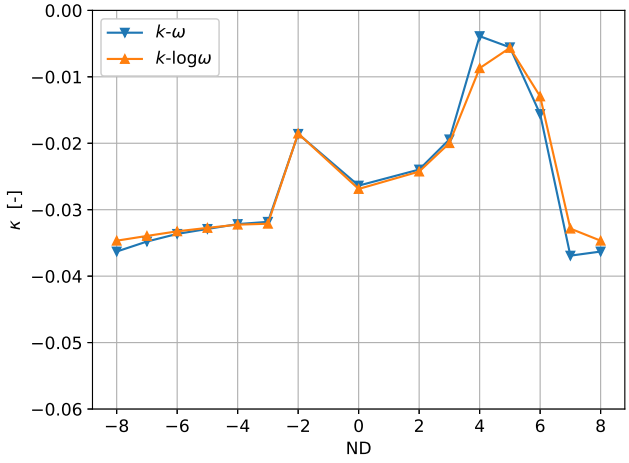

(b) Stiffness

Figure 8: Aerodynamic damping ratio over nodal diameter for k-ω and k-logω-formulations.

stiffness. It can be seen that, while the log ω-reformulation has little impact on the flow response for a large range of nodal diameters, the values in the vicinity of $N_d = 5$ are more sensitive. The value for $N_d = 5$ even changes the sign. Figures 9 and 10 compare the damping ratio per area for $N_d = 5$ at pressure and suction sides. One can see that the choice of the turbulence model formulation affects both the positive damping zone near the leading edge and the negative damping zone on the upper part of the pressure side.

Figure 8 also compares TRACE results to those obtained by Pagès et al. [6]. As a first conclusion, we observe that the results here, no matter which formulation of the SST model is used, predict a spike in the aerodynamic curve at $N_d = 5$, though not as pronounced as in [6]. That the other values match so well, however, is remarkable, given that the steady flow in [6] is obtained with a different solver (elsA) and the unsteady flow response was predicted with a time-linearized solver (Turb'Lin [20, 21]), which is based on Kok's k-ω turbulence model [22]) rather than Menter's SST model.

For the vibration amplitude used in this section (0.05 mm), both the original and the log ω-formulation are robust. When the amplitude is increased by a factor of 10, only simulations with the log ω-formulation are stable.

4 Boundary Conditions

Until now, the analysis used only one harmonic in the rotor domain and nonreflecting boundary conditions. Since these are perfectly nonreflecting only if the flow is inviscid, has no radial component and no radial pressure gradients, numerical reflections are to some extent unavoidable for a real 3D case. To analyze the impact of the boundary conditions, we run, for the nodal diameters 3 to 6 further HB setups. First, the computational domain is extruded at the inlet (cf. Fig. 1). This way we obtain an additional stationary domain where we prescribe the background flow fields with values extracted from the original inlet. This way we enforce identical flow fields in the rotor domain, thereby circumventing the difficulty of finding equivalent boundary values for the turbulence quanti-

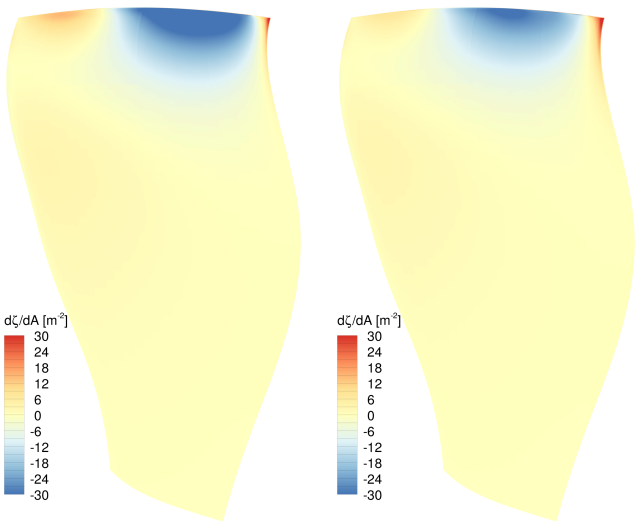

(a) k-ω (b) k-log ω

Figure 9: Aerodynamic damping ratio per area for $N_\mathrm{d} = 5$ at pressure side for k-ω and k-log ω-formulations.

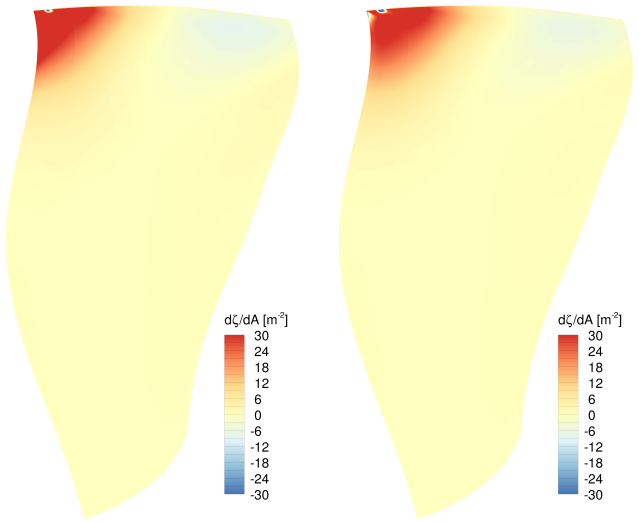

(a) k-ω (b) k-log ω

Figure 10: Aerodynamic damping ratio per area for $N_\mathrm{d} = 5$ at suction side for k-ω and k-log ω-formulations.

ties at a further upstream position. It is now possible in the HB solver to switch on additional modes in this entry section to propagate the disturbances from the rotor domain. This way, we compare the original result, with presumably some numerical reflections at the inlet, to a result with numerical reflections further upstream. The comparison of the damping and stiffness values is shown in Fig. 11.

Moreover, we perform a similar comparison to estimate the impact of reflections with the fan outlet: a harmonic corresponding to the eigenfrequency in the rotor system and the mode order given by the nodal diameter of the blade vibration is simulated in the stator domain. Note, however, that this configuration will not only shift the location of numerical reflections but also simulate the interaction with the OGV. The results have been added to the plot in Fig. 11. Both damping and stiffness vary significantly when the computational domain in which the unsteadiness is resolved is enlarged. In particular, the influence of the upstream boundary condition has a significant impact at the nodal diameter of 6 which is close to the cut-on/cut-off boundary for the inflow, cf. [6]. Similarly, the influence of the OGV domain can be seen, through less pronounced, for the nodal diameter of 4 which was found by Pagès et al. [6] to be very near the cut-on/cut-off boundary for the outflow.

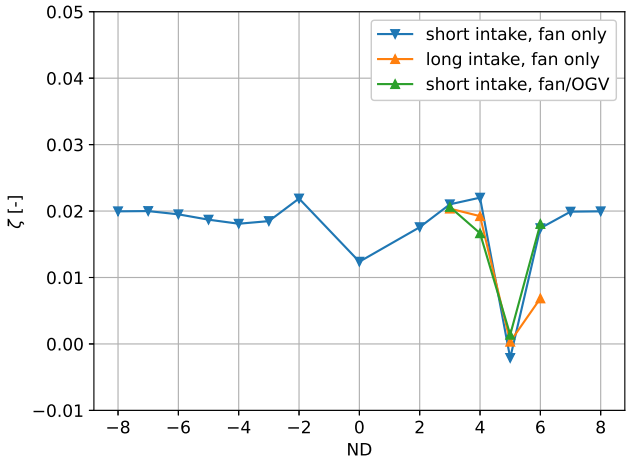

(a) Damping

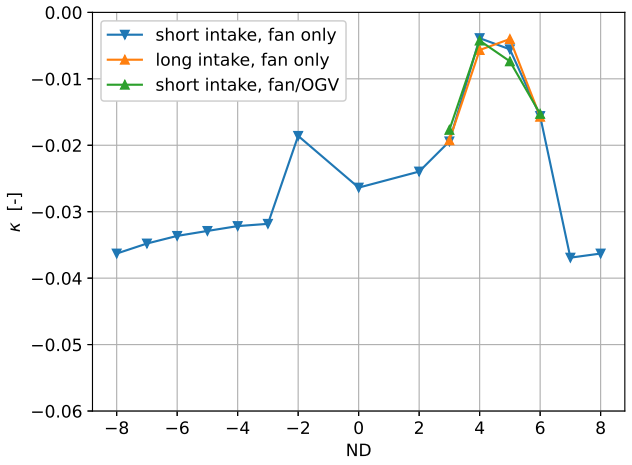

(b) Stiffness

Figure 11: Aerodynamic damping and stiffness ratios over nodal diameter for simulations with short and long inlet as well as interaction with OGV.

Regarding the spike at nodal diameter 5, however, reflections at the boundaries and interactions with the OGV seem insufficient to explain the sudden drop of the damping. Recall from Eqns. (1) and (2) that damping and stiffness together represent the complex aerodynamic work. Since the stiffness is not very sensitive either, we can therefore exclude the possibility that it is solely due to the phase of the reflected mode that the modal force due to the reflection has little impact on

the damping for the nodal diameter of 5.

The results above indicate that the aerodynamic damping computed in this work will have a significant uncertainty near the cut-on/cut-off boundaries due to the inlet and outlet boundary conditions. Away from these points, their impact seems limited. Note that, apart from numerical reflections, interactions with the intake may also alter the flutter characteristics [23, 24]. This phenomenon, however, is not studied here, the ideal flow solution would be one on a domain with infinitely long entries and exits.

5 Near Resonance Frequency

As was suspected by Pagès et al. [6], the spikes in the damping curve could indicate a resonance with a convective disturbance that travels with a particular relative circumferential speed $\dot{\vartheta}_c$. For a blade vibration with angular frequency ω and nodal diameter N_d to be in resonance with such a disturbance,

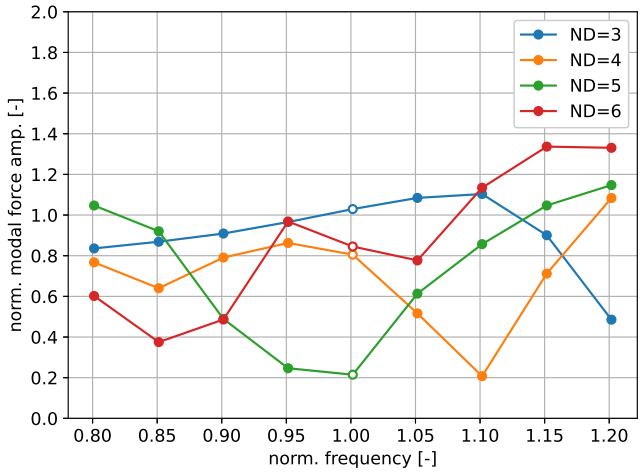

(a) Amplitude

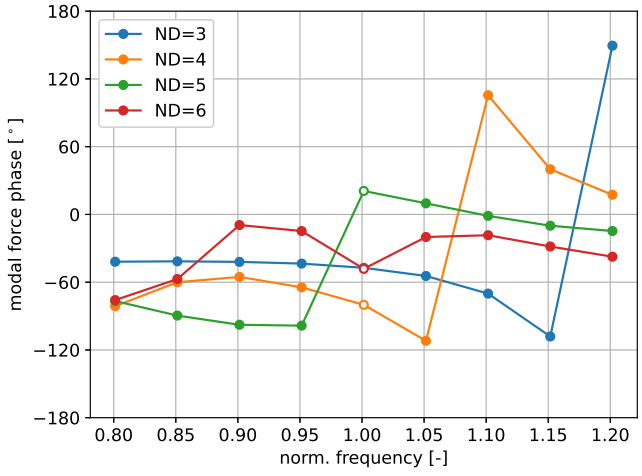

(b) Phase

Figure 12: Modal force amplitude and phase over frequency for different nodal diameters.

the condition

$$\dot{\vartheta}_c = -\frac{\omega}{N_d + lN} \tag{7}$$

with some integer l has to be satisfied. This convective disturbance must have the angular frequency ω and the circumferential mode order equal of $N_d + lN$.

As previous studies have shown [25], small disturbances can separate from the leading edge and travel, in the rotating frame of reference, with a specific speed in the range of -0.45 and -0.4 times the fan rotational speed. For the given eigenfrequency and a resonance near $N_d = 5$ the only value for l to give circumferential speeds in this range is $l = -1$.

To determine possible convective resonance frequencies, the eigenfrequency for the nodal diameters 3 to 6 has been varied ranging from -20% to $+20\%$ with steps of 5%. The resulting aerodynamic modal force over frequency, the latter normalized with the orginal one, is shown in Fig. 12. Here, the modal force is shown in terms of its amplitude and phase, as these are more appropriate to study the frequency response of an externally excited system near resonance. For instance, a forced mass-spring-damper system exhibits a sudden phase change near the resonance frequency. Note that a phase in the range between 0° and 180° indicates a negative aerodynamic damping. Especially for the nodal diameters 3, 4, and 5, one obtains a sudden change in the phase. The phase of the flow response here, at least in terms of the aerodynamic force, is thus reminiscent of that of a forced mass-spring-damper system near resonance.

To understand the location of the sudden phase changes, one can relate the frequency to a corresponding circumferential speed via Eq. (7) with $l = -1$. The same results as in Fig. 12 but over this potential resonance rotational speed are shown in Fig. 13. With the given numerical setup, resonance can be seen to occur at a relative rotation speed of -0.41Ω. Note also that the nodal diameters 3 and 4 with an appropriate increase of the eigenfrequency (10% and 20%, respectively) change from stable to unstable.

6 Nonlinear Flow Response

Until now, the flutter analysis has been based on the assumption that the flow response to the blade vibration is linear. Pagès et al. [6] point out that the unsteady solution that is obtained with their time-linearised solver for $N_d = 5$ yields implausibly high pressure amplitudes even for a relatively small vibration amplitude. It can therefore be suspected that, if those flow responses were valid for infinitesimal amplitudes, then, for the displacements considered here, nonlinear effects would have to set it. We therefore address in this section the question about the applicability of the linearisation hypothesis. Note that harmonic balance is particularly suited to study nonlinearity as it is, in the limit of infinitely many harmonics, capable of reproducing stable periodic solutions of the nonlinear system [26]. As mentioned above, the $\log\omega$-formulation of the SST model is used for this purpose.

It has been observed that when nonlinear effects set in, these have a considerable impact on the time-averaged fan outflow. Simulations with the isolated fan and a given pres-

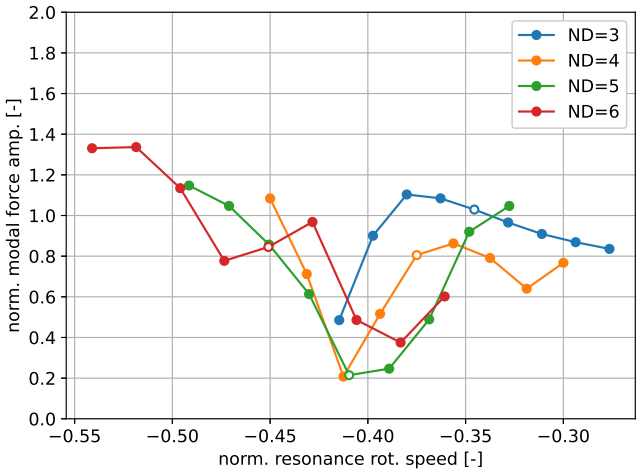

(a) Amplitude

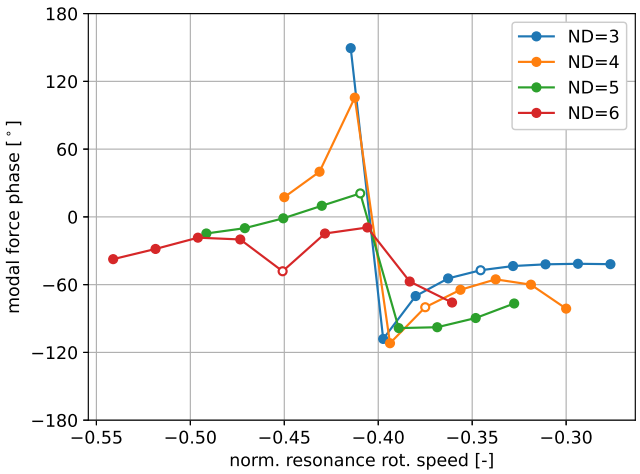

(b) Phase

Figure 13: Modal force amplitude and phase over convective speed of a disturbance which would be in resonance.

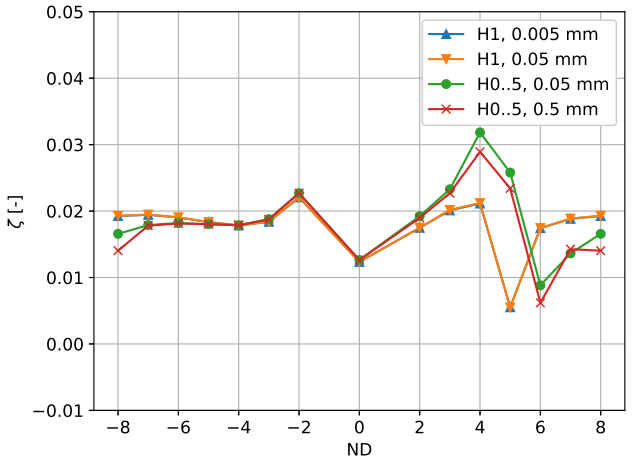

(a) Damping

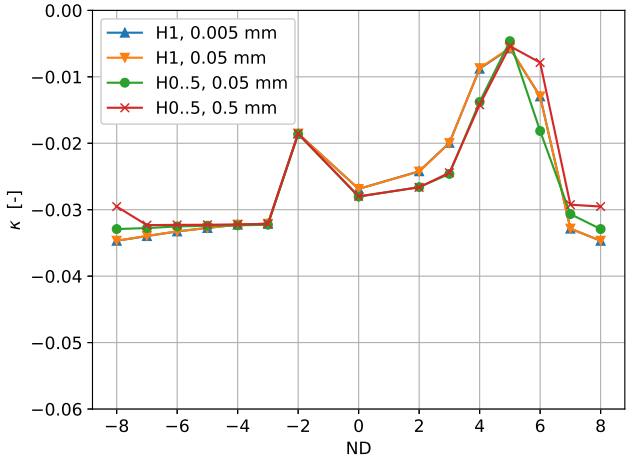

(b) Stiffness

Figure 14: Aerodynamic damping and stiffness ratios over nodal diameter for different harmonic sets and amplitudes.

sure profile at its outlet showed significant shifts of the operating point. Therefore, the following results were obtained on a computational domain that included the stator domain with the nozzle. The flow in the stator domain is resolved with the 0th harmonic only, its major role being that of a mass flow controller. Hence, no effects of a possible vane reflection or nonlinear mechanisms in the OGV domain are taken into account here.

We focus here on three questions about the aerodynamic damping and stiffness ratios:

Q1 What is the dependence on the vibration amplitude?

Q2 At what amplitudes do higher harmonics play a role?

Q3 What is the impact on the mean flow?

Due to the setup chosen in the previous sections ("HB1"), all effects related to questions Q2 and Q3 were suppressed by the approach. Note, however, that regarding Q1, there will possibly be a nonlinear amplitude dependence in the HB1-simulations as the flow residuals are not linearised. A flutter analysis with a reduced amplitude and just the first harmonic (H1), however, shows almost no change in damping and stiffness. The results for an amplitude of 0.005 mm are shown in Fig. 14. There is practically no dependence on the amplitude which demonstrates that the results in the previous sections were obtained for amplitudes still in the linear regime.

The flutter analysis has also been repeated with an HB setup that solves for the mean flow and five higher harmonics (HB0..5). Here, we have run the original displacement amplitude and one that was increased by a factor of 10. The results have been added to Fig. 14. For the nodal diameter of 3, 4 and 5, the aerodynamic damping is significantly higher for the HB0..5 setups while there is little difference for the negative nodal diameters. Most strikingly, the spike at $N_\mathrm{d} = 5$ seems to have shifted to the right and the minimum damping is now located at $N_\mathrm{d} = 6$.

To understand the nonlinear mechanisms behind the shift for nodal diameters close to 5, two further HB setups without blade vibration but with the interblade phase angle and frequency corresponding to the flutter analysis for $N_\mathrm{d} = 5$ were

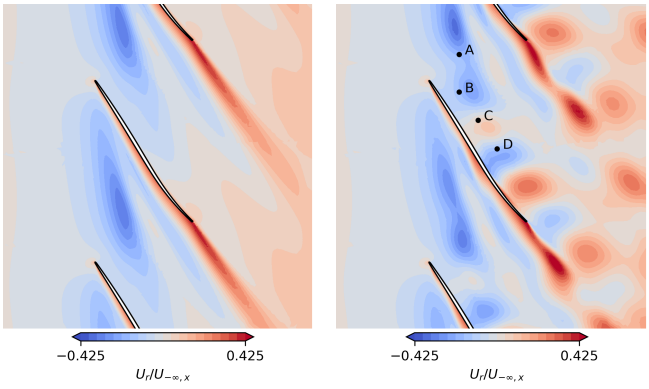

(a) Steady (b) HB0..5, instantaneous

Figure 15: Radial velocity at 95% channel height. Steady and HB with five harmonics but fixed blade.

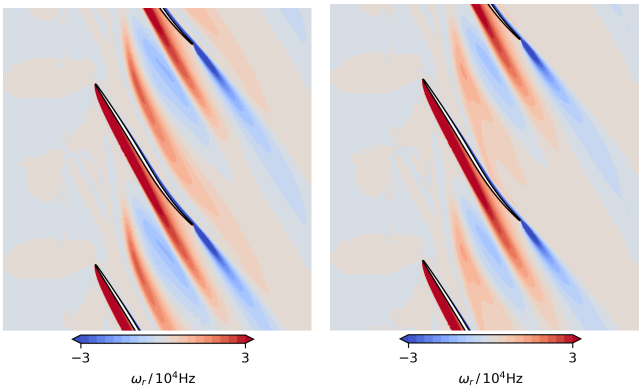

(a) Steady (b) HB0..5, time mean

Figure 16: Radial vorticity at 95% channel height. Steady and HB with five harmonics but fixed blade.

run: one with five (HB0..5) and one with 10 higher harmonics (HB0..10). Both simulations were initialised with the result for the vibration amplitude of 0.05 mm. It turns out that, rather than return to a steady flow, the harmonic balance solver then seems to approach a limit cycle. The plot in Fig. 15 compares the steady solution with a snapshot that was reconstructed from the HB0..5 solution. Note that for self-induced flow instabilities harmonic balance solvers tend to approach a limit cycle as has been observed by several authors, see e.g. the work of Spiker [27]. Figure 16 shows the impact of the unsteadiness on the mean flow in terms of the radial vorticity. The plot compares the steady solution to the time averaged result of the HB0..5 simulation and shows that the self-induced flow instability has a strong influence on the mean flow.

The spectrum of the entropy at the four numerical probes indicated in Fig. 15 is shown for the HB0..5 and the HB0..10 simulations in Fig. 17. Although no harmonic convergence is seen, both simulations have a clear concentration of the harmonic content in the fifth harmonic (and the 10th). Note that the k-th higher harmonic has k times the first interblade phase angle. Therefore, the phase relation between neighbouring passages by definition corresponds to the same time lag between passages and thus to identical circumferential speeds. It should be pointed out, however, that the frequency is held fixed even though for a self-sustained flow instability it is part of the unsteady flow problem. These convective disturbances should therefore be investigated in future studies using either time-domain simulations or harmonic balance methods with a frequency estimation and adaption.

Furthermore, for the HB0..5 setups the influence of the amplitude is relatively small, see Fig. 14. Figures 18 and 19 compare the damping ratio per area for $N_\mathrm{d} = 5$ at pressure and suction sides for the original and the higher vibration amplitudes. The figures show that there is practically no sensitivity to the amplitude. The flow response to the blade vibration, both globally and locally, is thus nearly linear in the amplitude. Note also the differences between these results and the ones for the H1 setups (Figs. 9 and 10). A possible explanation for this behaviour could be that, although the flow response to the blade vibration itself is a linear problem, the underlying background flow is already unsteady. This raises the question whether the discrepancy between the H1 and HB0..5 setups can be explained to large part with the fact that the mean flow changes due to the nonlinear effects. The plot in Fig. 20 compares the convergence of the aerodynamic damping ratio for various setups and nodal diameter 5. Here, “unst. mean” (solid green line) denotes an H1 setup where the frozen mean flow is taken as the time-average of the HB0..5 result with the standard amplitude (orange dashed line). On the one hand, the results do show, that the unsteady mean flow has a significant impact on the damping in that a flutter analysis with this background flow predicts a damping ration well above 1%. This effect, on the other hand, is insufficient to explain the full discrepancy between the “fully unsteady” flutter simulations and the original HB1 setup.

The plot in Fig. 14 shows that the resonance nodal diameter has been shifted to the right by taking into account the unsteady background flow. A shift from $N_\mathrm{d} = 5$ to 6, in turn, would mean a shift of the convective resonance mode order from -11 to -10, hence an increase of the relative circumferential convection speed by about 9%. Note that this would correspond to a relative rotation speed of about -0.45Ω, which is exactly the value that Fiquet et al. [7] observed for a time-domain URANS simulation with fixed blades. Very similar values for the relative rotation speed and a nodal diameter of 10 have been observed experimentally by Brandstetter et al. [28], though at a mass flow of $23.6\,\mathrm{kg\,s^{-1}}$. Tharreau et al. [29] recently found values near -0.41Ω at a mass flow of about $24.5\,\mathrm{kg\,s^{-1}}$ by means of time-domain CFD and reported a high sensitivity with respect to the tip gap height.

Conclusions

The flutter analysis of the UHBR Open Fan Testcase ECL5 CATANA was successfully conducted with the harmonic balance method and focused on the second eigenmode at part speed where previous computational studies at Ecole Centrale de Lyon showed negative damping for the nodal diameter 5. The simulation strategy employed here corresponds to the standard approach in that the unsteady flow due to a

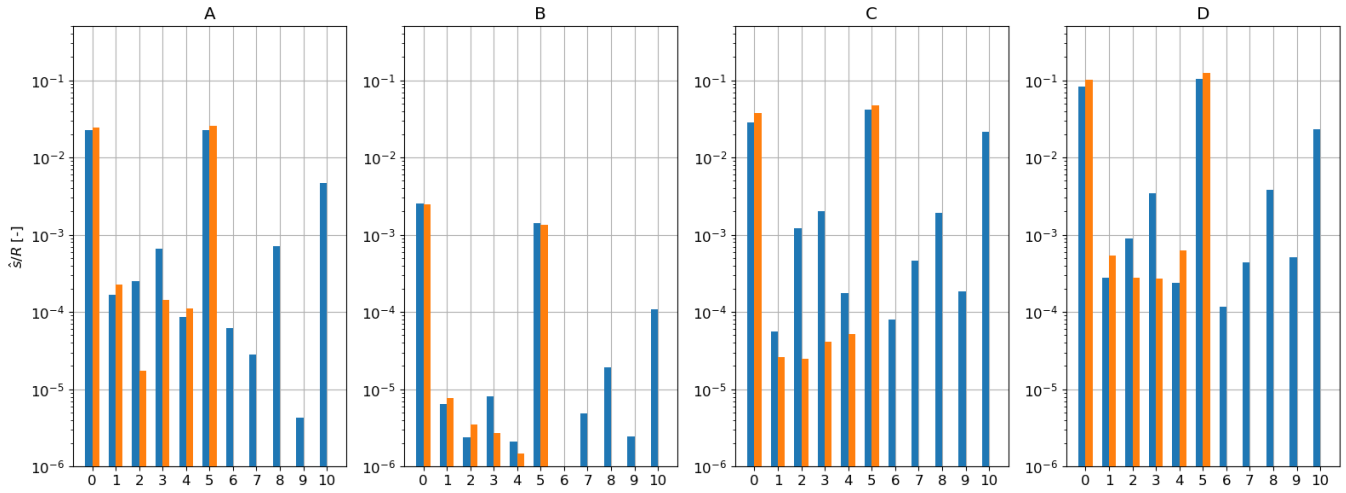

Figure 17: Spectrum of entropy for HB simulations with fixed blades at four points at 95% radial height.

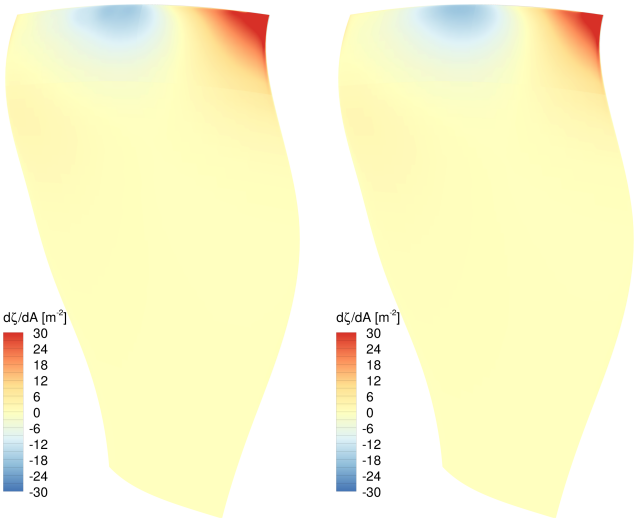

(a) 0.05 mm (b) 0.5 mm

Figure 18: Aerodynamic damping ratio per area for $N_d = 5$ at pressure side for H0..5 setups and different vibration amplitudes.

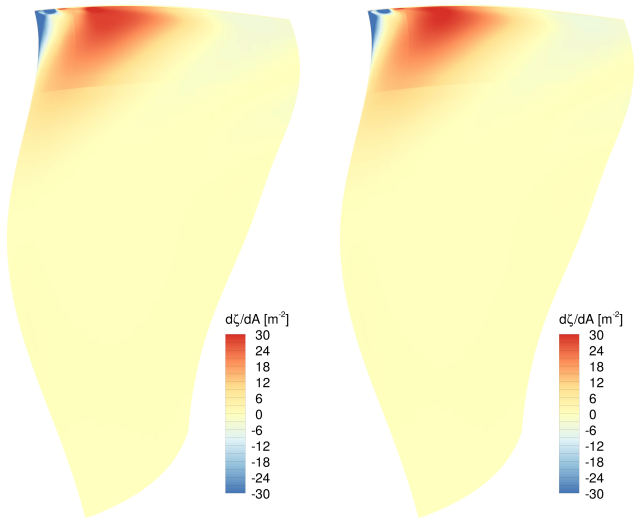

(a) 0.05 mm (b) 0.5 mm

Figure 19: Aerodynamic damping ratio per area for $N_d = 5$ at suction side for H0..5 setups and different vibration amplitudes.

harmonic blade vibration with prescribed frequency and interblade phase angle is computed, the main difference with the study at Ecole Centrale being that the frequency domain method here is nonlinear. At the operating point under consideration, the turbulence model quantities had to be modelled as unsteady. A test with frozen turbulence resulted in unsatisfactory convergence and unphysical flow solutions. The harmonic balance method turned out to be robust even for higher amplitudes when combined with the log ω-formulation of Menter's SST model.

Convergence varied significantly over the range of nodal diameters. For the nodal diameter 5 the aerodynamic damping was drifting slowly over a long period of iterations before convergence criteria were fulfilled. Apart from the HB method, the setup here differed from the above-mentioned study in that 2D nonreflecting boundary conditions were used. It was observed that the damping values, in particular at nodal diameters near the cut-on/cut-off boundary, have a high uncertainty due to possible numerical reflections.

The first part of our study employed a harmonic balance setup with a prescribed mean flow where only the first harmonic is predicted by the HB method. This approach resembles time-linearised methods. The agreement of the aerodynamic damping values predicted here with the previous study is quite high. The value for the nodal diameter of 5 was predicted much smaller than the other nodal diameters resulting in a V-shaped spike in the damping curve. This is in line with the results from ECL though the spike here was less pronounced. The depth of the spike was also found to be highly sensitive. Replacing the ω-equation with an equivalent log ω-

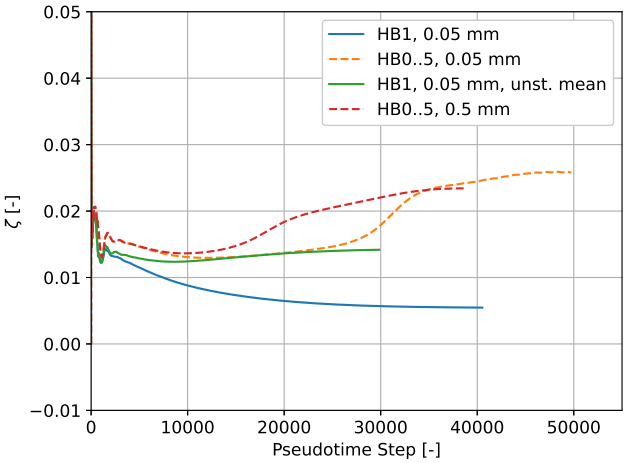

Figure 20: Aerodynamic damping over pseudotime step for $N_d = 5$. Setups with and without blade vibration.

formulation, for instance, caused a sign change of the damping. It can be concluded that when the harmonic configuration is as close as possible to the time-linearised setup then the damping values as well as the location of the spike (though not its depth) are in line with the results of the previous study.

A frequency sensitivity study revealed sudden phase changes of the complex aerodynamic modal force at certain frequencies depending on the nodal diameter. These could be related to a resonance with a convective disturbance the circumferential speed of which, in the relative frame of reference, is close to -0.41 times the fan rotational speed.

To understand the role of nonlinear mechanisms, the flutter analysis was repeated with a fully unsteady harmonic setup, solving for the mean flow and 5 higher harmonics. This setup gave significantly different damping values for nodal diameters close to 5. The aerodynamic damping at $N_d = 5$ increased considerably and was well above 1%. This is in line both with experiments where high amplitudes for $N_d = 5$ were not observed and with computational studies by Fiquet et al. [7] which predicted a damping ratio of about 1.5%. Adding harmonics to the harmonic balance setups can therefore help to explain the discrepancy and apparent contradiction between the published linear and nonlinear results.

The change in the damping between "linear" and nonlinear approaches has been found to be, at least to some extent, due to the fact, that the unsteady flow is erroneously linearised at the steady solution. When running the testcase with sufficiently many harmonics, the HB solver, as did time-domain solvers in [7] resolves an unsteadiness which is present even if the blades are held fixed. In contrast, the numerical dissipation of the pseudotime scheme used to compute the steady flow, in combination with periodic boundaries, seems to prevent the onset of this convective disturbance. We conclude that to obtain physically meaningful damping values, it is indispensable to resolve the convective disturbances related to NSV and its impact on the mean flow. Moreover, time-domain simulations with fixed blades and numerical setups consistent with the ones used here, are planned to shed more light on the nature of these flow instabilities.

Acknowledgements

A large part of this study was carried out during a stay of the first author at the LMFA of the Ecole Centrale de Lyon. He would like to thank the whole team in Lyon for their warm welcome, the support and fruitful discussions. Financial support from DLR's Institute of Propulsion Technology is also acknowledged.

Nomenclature

Roman symbols

f	frequency
f_{eigen}	eigenfrequency
F_{mod}	modal force
k	harmonic index
K	number of non-zero harmonics
$\vec{n}$	surface normal (pointing out of the fluid domain)
N	blade count
N_d	nodal diameter
N_{sp}	number of sampling points
p	static pressure
q	flow state
q_s	displacement
R	flow residual
U	relative velocity
V	cell volume
W_{cyc}	aerodynamic work per cycle

Greek symbols

Γ	blade surface
ζ	aerodynamic damping ratio
ϑ	circumferential coordinate
κ	aerodynamic stiffness ratio
Ψ	mode shape
ω	angular frequency
ω	turbulence dissipation rate
Ω	rotor angular velocity

Subscripts

c	convective
mod	modal
r	radial

Superscripts

$\dot{}$	time derivative
$\hat{}$	harmonic

Acronyms

CFD	computational fluid dynamics
HB	harmonic balance
rpm	revolutions per minute
TM	turbulence model

References

[1] I. J. Day. "Stall, Surge, and 75 Years of Research". In: *Journal of Turbomachinery* 138.1 (2015), p. 011001. DOI: 10.1115/1.4031473.

[2] R. E. Kielb, J. W. Barter, J. P. Thomas, and K. C. Hall. "Blade Excitation by Aerodynamic Instabilities: A Compressor Blade Study". In: 36878. 2003, pp. 399–406. DOI: 10.1115/GT2003-38634.

[3] S. Stapelfeldt and C. Brandstetter. "Non-synchronous vibration in axial compressors: Lock-in mechanism and semi-analytical model". In: *Journal of Sound and Vibration* 488 (2020). DOI: 10.1016/j.jsv.2020.115649.

[4] A. Srinivasan. "Flutter and Resonant Vibration Characteristics of Engine Blades". In: *Journal of Engineering for Gas Turbines and Power* 119 (1997), pp. 742–775.

[5] M. Vahdati and N. Cumpsty. "Aeroelastic Instability in Transonic Fans". In: *Journal of Engineering for Gas Turbines and Power* 138.2 (2015), p. 022604. DOI: 10.1115/1.4031225.

[6] V. Pagès, P. Duquesne, S. Aubert, L. Blanc, P. Ferrand, X. Ottavy, and C. Brandstetter. "UHBR Open-Test-Case Fan ECL5/CATANA". In: *International Journal of Turbomachinery, Propulsion and Power* 7.2 (2022). DOI: 10.3390/ijtpp7020017.

[7] A.-L. Fiquet, A. Schneider, B. Paoletti, X. Ottavy, and C. Brandstetter. "Experiments on the Tuned UHBR Open-Test-Case Fan ECL5/CATANA: Stability Limit". In: vol. 11A. 2023. DOI: 10.1115/GT2023-102537.

[8] A.-L. Fiquet, X. Ottavy, and C. Brandstetter. "UHBR Open-Test Case Fan ECL5/ CATANA: Non-Linear Analysis of Non-Synchronous Blade Vibration at Part-Speed Conditions". In: *Journal of Turbomachinery* 146.7 (2024). DOI: 10.1115/1.4064841.

[9] F. Menter, M. Kuntz, and R. Langtry. "Ten years of Industrial experience with the SST model." In: *Turbulence, Heat and Mass Transfer 4*. Ed. by K. Hanjalić, Y. Nagano, and M. Tummers. 2003.

[10] M. Kato and B. E. Launder. "The Modeling of Turbulent Flow Around Stationary and Vibrating Square Cylinders". In: *9th Symposium on Turbulent Shear Flows*. 1993, pp. 10.4.1–10.4.6.

[11] P. L. Roe. "Approximate Riemann solvers, parameter vectors, and difference schemes". In: *J. Comput. Phys.* 43.2 (1981), pp. 357–372. ISSN: 0021-9991. DOI: 10.1016/0021-9991(81)90128-5.

[12] B. van Leer. "Towards the ultimate conservative difference scheme. V. A second-order sequel to Godunov's method". In: *J. Comput. Phys.* 32.1 (1979), pp. 101–136. ISSN: 0021-9991. DOI: 10.1016/0021-9991(79)90145-1.

[13] G. D. van Albada, B. van Leer, and W. W. Roberts Jr. "A comparative study of computational methods in cosmic gas dynamics". In: *Astron. Astrophys.* 108.1 (1982), pp. 76–84.

[14] C. Frey, G. Ashcroft, H.-P. Kersken, and C. Voigt. "A Harmonic Balance Technique for Multistage Turbomachinery Applications". In: *ASME Turbo Expo 2014: Turbine Technical Conference and Exposition*. 45615. 2014, V02BT39A005. DOI: 10.1115/gt2014-25230.

[15] G. Ashcroft, C. Frey, and H.-P. Kersken. "On the Development of a Harmonic Balance Method for Aeroelastic Analysis". In: *6th European Conference on Computational Fluid Dynamics (ECFD VI)*. 2014, pp. 5885–5897.

[16] C. Frey, G. Ashcroft, H.-P. Kersken, and D. Schlüß. "Flutter Analysis of a Transonic Steam Turbine Blade with Frequency and Time-Domain Solvers". In: *International Journal of Turbomachinery, Propulsion and Power* 4.2 (2019). ISSN: 2504-186X. DOI: 10.3390/ijtpp4020015.

[17] J. P. Heners, D. M. Vogt, C. Frey, and G. Ashcroft. "Investigation of the impact of unsteady turbulence effects on the aeroelastic analysis of a low-pressure turbine rotor blade". In: *Journal of Turbomachinery* (2019), pp. 1–12. ISSN: 0889-504X. DOI: 10.1115/1.4043950.

[18] M. Müller, H.-P. Kersken, and C. Frey. "A Log-w Turbulence Model Formulation for Flutter Analysis with Harmonic Balance". In: *16th International Symposium on Unsteady Aerodynamics, Aeroacoustics & Aeroelasticity of Turbomachines ISUAAAT16 (to appear)*. 2022.

[19] H.-P. Kersken, C. Frey, C. Voigt, and G. Ashcroft. "Time-Linearized and Time-Accurate 3D RANS Methods for Aeroelastic Analysis in Turbomachinery". In: *J. Turbomach.* 134.5 (2012), p. 051024. ISSN: 0889-504X. DOI: 10.1115/1.4004749.

[20] Q. Rendu, M. Philit, S. Labit, J.-C. Chassaing, Y. Rozenberg, S. Aubert, and P. Ferrand. "Time-Linearized and Harmonic Balance Navier-Stokes Computations of a Transonic Flow over an Oscillating Bump". In: *Proceedings of the 14th International Symposium on Unsteady Aerodynamics, Aeroacoustics & Aeroelasticity of Turbomachines ISUAAAT14*. 2015.

[21] M. Philit, P. Ferrand, S. Labit, J.-C. Chassaing, S. Aubert, and T. Fransson. "Derivated turbulence model to predict harmonic loads in transonic separated flows over a bump". In: *28th Congress of the International Council of the Aeronautical Sciences 2012, ICAS 2012* 4 (2012), pp. 2713–2723.

[22] J. Kok. *Resolving the Dependence on Free-stream Values for the K-omega Turbulence Model*. Tech. rep. NLR-TP-99295. Nationaal Lucht- en Ruimtevaartlaboratorium, 1999.

[23] F. Zhao, N. Smith, and M. Vahdati. "A simple model for identifying the flutter bite of fan blades". In: 139.7 (2017). DOI: 10.1115/1.4035567.

[24] T. Bontemps, S. Aubert, and M. de Pret. "Prediction of the Acoustic Reflection in a Realistic Aeroengine Intake With Three Numerical Methods to Analyze Fan Flutter". In: *Journal of Turbomachinery* 143.10 (2021). DOI: 10.1115/1.4051113.

[25] M. Rodrigues, L. Soulat, B. Paoletti, X. Ottavy, and C. Brandstetter. “Aerodynamic Investigation of a Composite Low-Speed Fan for UHBR Application”. In: *Journal of Turbomachinery* 143.10 (2021), p. 101004. DOI: 10.1115/1.4050671.

[26] C. Frey, J. Backhaus, G. Ashcroft, G. Geiser, B. Winhart, and H. Stueer. “Using Pseudotime Marching for the Solution of Harmonic Balance Problems”. In: *Journal of Turbomachinery* 147.9 (2025), p. 091007. DOI: 10.1115/1.4067519.

[27] M. A. Spiker. “Development of an Efficient Design Method for Non-synchronous Vibrations”. PhD thesis. Duke University, 2008.

[28] C. Brandstetter, A.-L. Fiquet, A. Schneider, B. Paoletti, and X. Ottavy. “Experiments on Tuned UHBR Open-Test-Case Fan ECL5/CATANA: Stability Limit”. In: *Journal of Engineering for Gas Turbines and Power* 146.5 (2024). DOI: 10.1115/1.4063717.

[29] P. Tharreau, M. Hardy-Falch, S. Stapelfeldt, and C. Brandstetter. “Non-Synchronous Vibration: Characterisation of the Aerodynamic Disturbance and its Dependency on Local Tip Clearance”. In: *Turbo Expo: Power for Land, Sea, and Air*. Vol. Volume 10A: Structures and Dynamics. 2024, V10AT21A021. DOI: 10.1115/GT2024-129186.